Guo, Jianpeng; Pulkkinen, Tuija I.; Tanskanen, E.I.; Feng, Xueshang; Emery, Barbara A.; Liu, Huixin; Liu, Chaoxu; Zhong, Dingkun

Annual variations in westward auroral electrojet and substorm occurrence rate during solar cycle 23

Published in:
Journal of Geophysical Research: Space Physics

DOI:
10.1002/2013JA019742

Published: 01/01/2014

Document Version
Publisher's PDF, also known as Version of record

AGU PUBLICATIONS

JGR

Journal of Geophysical Research: Space Physics

BRIEF REPORT

10.1002/2013JA019742

Key Points:
- Annual variations of WEJ in 2200–0100 MLT are associated with solar wind driving
- Annual variations of WEJ in 0300–0600 MLT are due to EUV and equinoctial effect
- Solar wind driving contributes to higher substorm occurrence in winter

Correspondence to:
J. Guo and X. Feng,
jpguo@spaceweather.ac.cn;
fengx@spaceweather.ac.cn

Citation:
Guo, J., T. I. Pulkkinen, E. I. Tanskanen, X. Feng, B. A. Emery, H. Liu, C. Liu, and D. Zhong (2014), Annual variations in westward auroral electrojet and substorm occurrence rate during solar cycle 23, *J. Geophys. Res. Space Physics*, *119*, 2061–2068, doi:10.1002/2013JA019742.

Received 26 DEC 2013
Accepted 27 FEB 2014
Accepted article online 4 MAR 2014
Published online 24 MAR 2014

Annual variations in westward auroral electrojet and substorm occurrence rate during solar cycle 23

Jianpeng Guo[1,2], T. I. Pulkkinen[3], E. I. Tanskanen[4,5], Xueshang Feng[1], Barbara A. Emery[6], Huixin Liu[2], Chaoxu Liu[1], and Dingkun Zhong[1]

[1]SIGMA Weather Group, State Key Laboratory of Space Weather, CSSAR, Chinese Academy of Sciences, Beijing, China, [2]Department of Earth and Planetary Sciences, Faculty of Sciences, Kyushu University, Fukuoka, Japan, [3]School of Electrical Engineering, Aalto University, Espoo, Finland, [4]Finnish Meteorological Institute, Helsinki, Finland, [5]Department of Physics and Technology, University of Bergen, Bergen, Norway, [6]High Altitude Observatory, NCAR, Boulder, Colorado, USA

Abstract The International Monitor for Auroral Geomagnetic Effects network magnetic measurements during the period 1995–2009 are used to characterize the annual variations in the westward electrojet. The results suggest that the annual variations in different local time sectors are quite different due to the different sources. In the MLT sector 2200–0100, the annual variations with maxima in winter suggest they are caused by the combined effects of the convective electric field and the conductivity associated with particle precipitation. Furthermore, the conductivity seems to play a more important role in the MLT sector ~2200–2320, while the convective electric field appears to be more important in the MLT sector ~2320–0100. In the MLT sector 0300–0600, the annual variations with maxima in summer suggest they are caused by solar EUV conductivity effect and the equinoctial effect. The solar EUV conductivity effect works by increasing ionospheric conductivity and enhancing the westward electrojet in summer, while the equinoctial effect works by decreasing solar wind-magnetosphere coupling efficiency and weakening the westward electrojet in winter. In the MLT sector 0100–0300, the annual variations are relatively weak and can be attributed to the combined effects of annual variations caused by all the previously mentioned effects. In addition, we find that a significant annual variation in substorm occurrence rate, mainly occurring in the premidnight region, is quite similar to that in the westward electrojet. We suggest that elevated solar wind driving during the winter months contributes to higher substorm occurrence in winter in the Northern Hemisphere.

1. Introduction

The auroral electrojets are mostly Hall currents flowing approximately in the auroral oval, mainly as an eastward current in the dusk sector and a westward current in the midnight and dawn sectors. Occasionally, the westward electrojet is fed by the closure of the substorm current wedge [*Newell and Gjerloev*, 2011] and shows an extra enhancement in the midnight sector. Both the eastward electrojet and the westward electrojet are controlled by the convection electric field and the Hall conductivity over the region [*Ahn et al.*, 1999, 2000]. The convection electric field is mainly produced by the interaction between the solar wind and magnetosphere in terms of reconnection and viscous interaction. Thus, the convection electric field variability is closely associated with the interplanetary magnetic field (IMF) *By* and *Bz* components and solar wind speed [see *Weimer*, 1996, 2005; *Ridley et al.*, 2000; *Matsuo et al.*, 2002]. There are two sources of ionospheric conductivity: one is associated with the solar EUV radiation varying smoothly and maximizing near local noon and the other with auroral particle precipitation, which shows a maximum around local midnight [see *Ahn et al.*, 1999, 2000; *Guo et al.*, 2012].

Since the auroral electrojet indices (*AU*, *AL*, and *AE*, hereafter called the *AE* indices) were introduced by *Davis and Sugiura* [1966] for routine monitoring of the ionospheric currents in the auroral oval region, they have been widely used to study the seasonal variations in the auroral electrojets [e.g., *Russell and McPherron*, 1973; *Svalgaard*, 1977; *Ahn et al.*, 2000; *Cliver et al.*, 2000; *Lyatsky et al.*, 2001; *Newell et al.*, 2002; *Zhao and Zong*, 2012; *McPherron et al.*, 2013]. The results suggest that the eastward electrojet shows an annual variation with maximum during the summer months and minimum during the winter months, and the westward electrojet shows a semiannual variation with maxima in the spring and fall. More recently, to examine whether some of seasonal variations in the *AE* indices are due to the sparse distribution of the AE stations,

Singh et al. [2013] analyzed the SuperMAG electrojet (SME) indices derived from more than 70 magnetometer stations during the period 1997–2009 [*Newell and Gjerloev*, 2011] and found that the SME indices exhibit similar seasonal variations as those observed in the *AE* indices. So they concluded that most of the observed seasonal variations in the *AE* indices are mainly due to the actual physical processes that control them.

All of the above studies provided little information of magnetic local time (MLT) dependence of seasonal variations of auroral electrojet activity. The auroral electrojets derived from a meridional magnetometer chain, such as the International Monitor for Auroral Geomagnetic Effects (IMAGE) magnetometer chain, can be used to address this issue. When the IMAGE chain rotates into a local time sector (~2 h), it can monitor the auroral electrojet activity in its corresponding sector [*Kauristie et al.*, 1996; *Pulkkinen et al.*, 2011; *Guo et al.*, 2012]. Thus, the IMAGE chain can provide information about the MLT variations of the auroral electrojets after it finishes scanning all local time sectors. In this paper, we analyze the westward electrojet parameters derived from the IMAGE chain to characterize the seasonal variations in the westward electrojet during the period 1995–2009. As expected, the westward electrojet shows significant MLT dependence in the seasonal variations, particularly in the annual variation. The primary objective of the present study is to investigate the cause of the annual variation in the westward electrojet in the midnight and dawn sectors (roughly 2200–0600 MLT). In addition, considering that the occurrence rate of substorms observed by the IMAGE magnetometer network also shows a significant annual variation [*Tanskanen et al.*, 2011], we will investigate the relationship between the annual variations in the westward electrojet and the substorm occurrence rate, as well as the potential implications.

2. IMAGE Data

The IMAGE chain consists of 31 magnetometers ranging in latitude from 58° (Tartu, Estonia) to 79° (Ny-Ålesund, Svalbard) or from 54° to 75° in corrected geomagnetic coordinates [*Tanskanen*, 2009]. The stations have longitudinal coverage over about 30° from western Norway to the Kola peninsula. The MLT sectors corresponding to the IMAGE chain are approximately 2 h later of UT. The IL index and total westward electrojet current (WEJ) determined from the IMAGE magnetic measurements during the period 1995–2009 are used for this study. The IL index is the envelope curve of the north-south component of the magnetic field computed in the similar way to the global *AL* index, and it is intended to express the strongest westward current intensity [*Kallio et al.*, 2000]. WEJ is processed using the derivation procedures of *Amm and Viljanen* [1999] and *Pulkkinen et al.* [2003]. Note that when the IMAGE chain is outside the MLT sector 2200–0600 (optimal MLT sector), the derived IL index and WEJ have limited accuracy [see *Kauristie et al.*, 1996; *Guo et al.*, 2012]. As we will see later, the IL index actually shows the same behavior as WEJ in the annual variations.

3. Results and Discussion

3.1. Annual Variation in Westward Electrojet

Lomb-Scargle periodograms [*Lomb*, 1976; *Scargle*, 1982] are calculated on daily IL index and WEJ in each MLT bin (1 min) to examine the large time scale (with the periods >27 days) seasonal variations from 1 January 1995 to 31 December 2009. This method has been selected over conventional Fourier methods because of its ability to handle unevenly sampled data or data with gaps (in fact only for short gaps). The corresponding results are shown in Figures 1a and 1b, respectively. Predominant spectral peaks can be found at the periods of ~180–190 and ~350–380 days, which correspond to semiannual variations and annual variations, respectively. The spectral peaks near 400 days are also present around 0100–0200 MLT. It is not immediately clear whether they are the signals of annual variations. We will discuss this later. The semiannual variation in geomagnetic and auroral activity has been recognized for a long time. One of the most prevailing explanations is the Russell and McPherron (R-M) effect [*Russell and McPherron*, 1973]. A related implication of the R-M effect is that in spring and fall, when the dipole axis is tilted perpendicular to the Earth-Sun line (the *x* axis in both GSE and GSM magnetic coordinates), an IMF *By* component in GSE converts to a *z* component in GSM. Thus, the equinoctial peak has often been attributed to GSE *By* partially converting to GSM *Bz* at equinoxes, thus producing a larger magnitude *Bz* on average around March and September. However, in many cases the R-M effect has not been able to explain the full seasonal and diurnal variations, which has led to the suggestions of an equinoctial effect [*Svalgaard*, 1977; *Cliver et al.*, 2000; *Finch et al.*, 2008; *Zhao and Zong*, 2012]. One explanation proposed for this is the effect of solar EUV conductivity

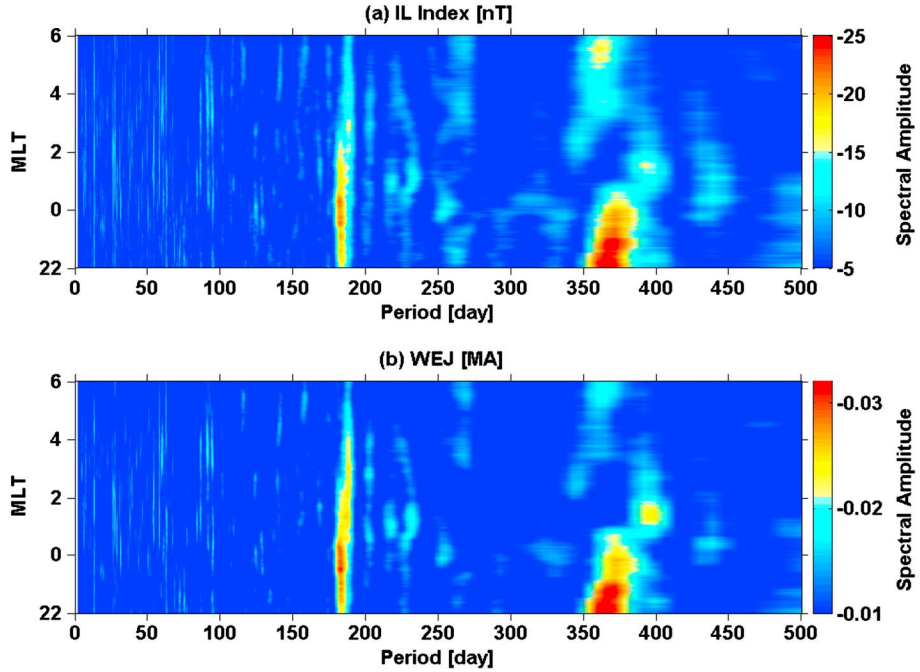

Figure 1. Contour plots of spectral amplitudes of (a) the IL index and (b) the total westward electrojet currents (WEJ) as a function of MLT and periods during 1995–2009.

changes on the auroral electrojet on the nightside [*Lyatsky et al.*, 2001; *Newell et al.*, 2002], acting in addition to the R-M effect. In this study, we will focus our investigation mainly on the annual variations and their sources in the westward electrojet.

In order to elucidate the annual variations, we apply a band-pass filter to each MLT bin of IL index and WEJ. The band-pass filter is centered at 365 days, with half-power points at 365 ± 20 days. Band-pass-filtered IL

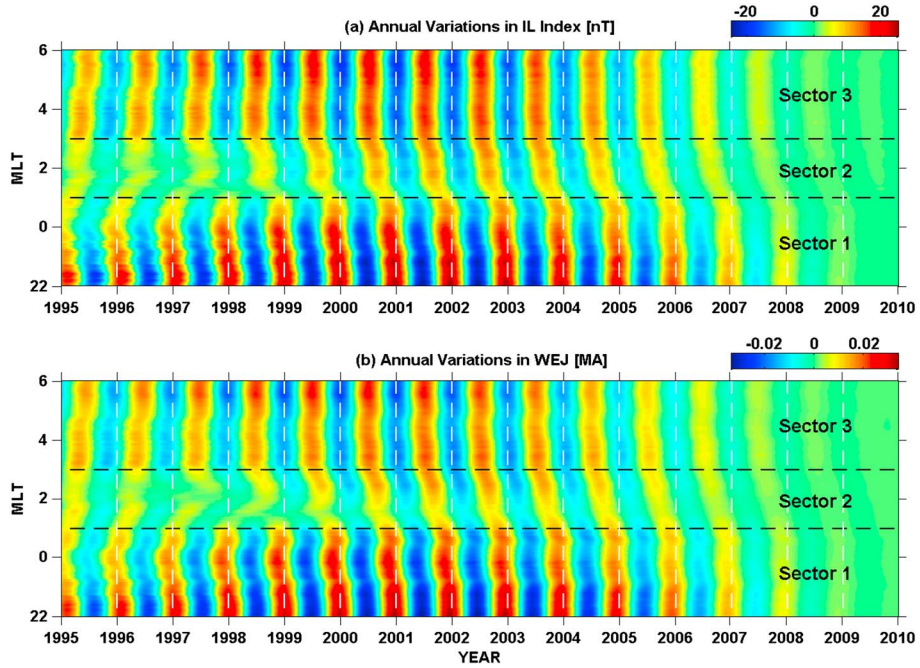

Figure 2. Band-pass-filtered annual variation of (a) the IL index, and (b) WEJ as function of MLT and day number during 1995–2009. The band-pass filter is centered at the period of 365 days, with half-power points at 365 ± 20 days. The vertical dashed lines show the beginnings of the years. The optimal MLT region is divided into three sectors (Sector 1: 2200–0100 MLT, Sector 2: 0100–0300 MLT, and Sector 3: 0300–0600 MLT) by two horizontal dashed lines.

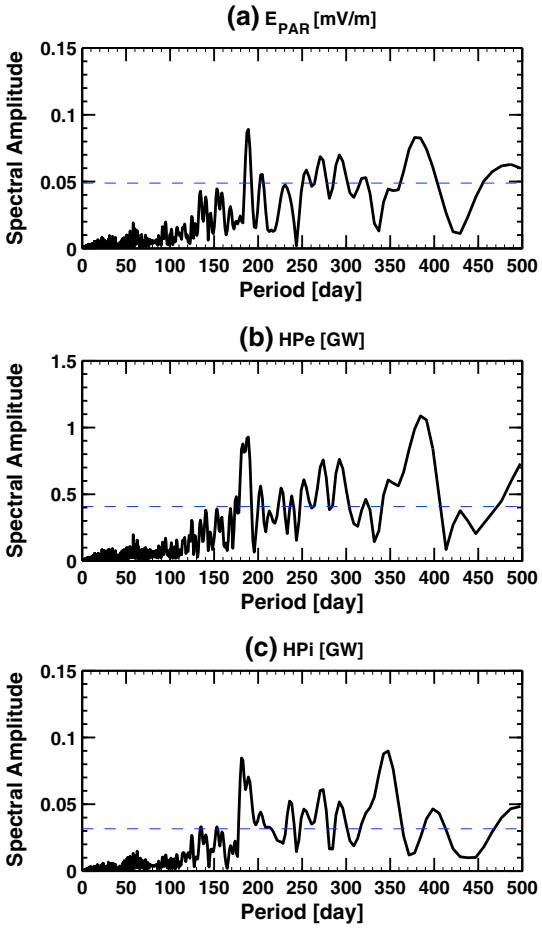

Figure 3. Lomb-Scargle spectral amplitudes of 27 day running means of (a) parallel electric field E_{PAR}, (b) HPe, and (c) HPi during 1995–2009. The horizontal dashed lines represent the 99% significance level.

index residuals and WEJ residuals are shown in Figures 2a and 2b, which reveal two interesting features: (1) the annual variations in the MLT sectors 2200–0100 (Sector 1) and 0300–0600 (Sector 3) are exceptionally strong, while those in the MLT sector 0100–0300 (Sector 2) are quite weak (cf. Figure 1) and (2) in Sector 1 the maximum occurs in winter months and minimum occurs in the summer months; and the opposite is true in Sector 3. This indicates that the annual variations in Sector 1 and Sector 3 might be caused by different drivers. One may easily associate the annual variations in Sector 3 with solar EUV conductivity effects. When the nightside oval in Northern Hemisphere is sunlit, ionospheric Hall conductivity during the summer months is enhanced by solar illumination, which can lead to higher Hall current. Because the Hall conductivity around midnight is mainly determined by particle precipitation, the annual variation in current caused by solar EUV may occur only in the dawn sector, as we have observed in Figure 2. It should be noted, however, that the nightside oval is only sunlit by a few degrees for a short period in the summer. Moreover, since the dawn sector is close to the terminator, the solar EUV induced conductivity is relatively low (<2 mho) [*Ridley et al.*, 2004]. For these reasons, solar EUV conductivity effect is insufficient to explain the observed annual variations. Here we propose that the equinoctial hypothesis is another potential mechanism [*Cliver et al.*, 2000], besides solar EUV conductivity effect. According to the equinoctial effect, when the angle Ψ between Earth-Sun line and the dipole axis of the Earth is further from 90°, the solar wind-magnetosphere coupling is less efficient and the geomagnetic activity is lower. During the period 01–03 UT, when the IMAGE chain scans Sector 3, the angle Ψ minimizes in winter [cf. *Cliver et al.*, 2000, Figure 1], which could result in the weaker westward electrojet. In fact, the equinoctial effect on the westward auroral electrojet has been reported by *Finch et al.* [2008]. In this way, we can explain the observed annual variations in IL and WEJ by solar EUV conductivity effect and the equinoctial effect, which work in two fundamentally different ways. The solar EUV conductivity effect works by increasing ionospheric conductivity and enhancing the westward electrojet in summer, while the equinoctial effect works by decreasing solar wind-magnetosphere coupling efficiency and weakening the westward electrojet in winter.

In the following, we will investigate the potential contributions of the convective electric field and the conductivity associated with particle precipitation to the observed annual variations in Sector 1, as well as their possible association with solar wind driving. We choose parallel electric field E_{PAR} as a solar wind driving function. The parallel electric field is defined as $E_{PAR} = E\sin(\theta/2)$, where E is the magnitude of the solar wind electric field computed as $-V \times B$ (V is the solar wind velocity and B is the IMF vector) and θ is the IMF clock angle. The component E_{PAR} gives the electric field component roughly along the large-scale neutral line at the magnetopause and thus is a measure of the reconnection efficiency at the dayside magnetopause [see *Pulkkinen et al.*, 2010]. Lomb-Scargle analysis is performed on 27 day running means of parallel electric field E_{PAR}, Northern Hemisphere (NH) electron hemispheric power (HPe), and NH ion hemispheric power (HPi) during 1995–2009 (Note: applying a running mean over a span of one solar rotation can suppress the short-term variations in these data). The solar wind magnetic field and plasma parameters used

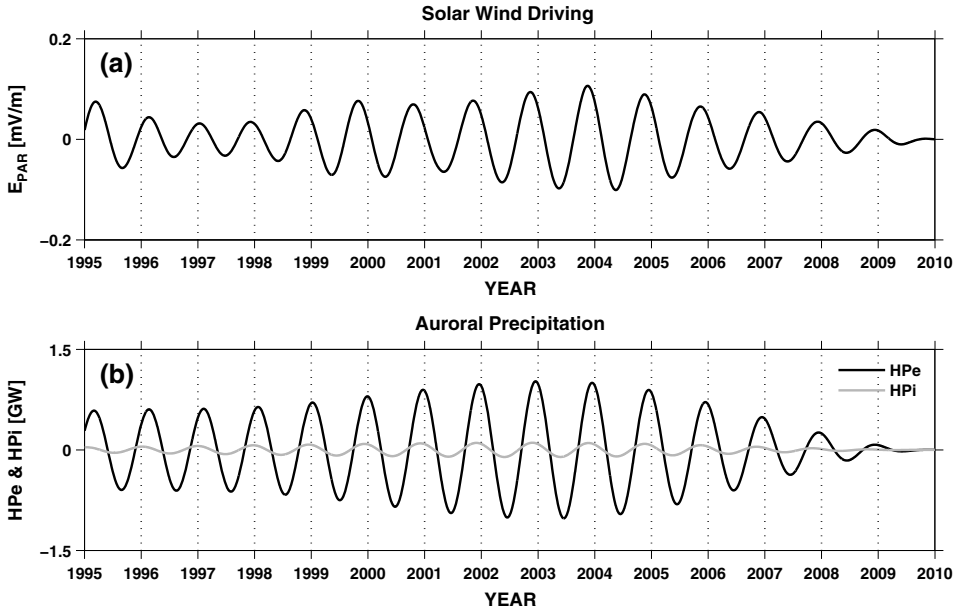

Figure 4. Band-pass-filtered annual variation of (a) solar wind driving (E_{PAR}) and (b) auroral particle precipitation (HPe and HPi) during 1995–2009. The band-pass filter is centered at the period of 365 days, with half-power points at 365 ± 20 days. The vertical dashed lines show the beginnings of the years.

for E_{PAR} calculation are available from the hourly OMNI data set and are averaged to daily values. Global auroral precipitation estimates on a 1 h cadence are computed by using data from Defense Meteorological Satellite Program and Polar Orbiting Environmental Satellites from the National Oceanic and Atmospheric Administration cross calibrated by *Emery et al.* [2008, 2009]. Considering the diurnal variations in auroral precipitation, the daily averages of HPe and HPi (< 20 keV) used here are calculated using only data from 2000–2300 UT, when the IMAGE chain scans the MLT sector 2200–0100 (Sector 1). The periodogram results are shown in Figure 3. Predominant spectral peaks can be seen at the periods of ~180–190 and ~350–400 days, which correspond to semiannual variations and annual variations, respectively. The semiannual variation in E_{PAR} is mainly due to the R-M effect (IMF *By* component in GSE converts to a *Bz* component in GSM at equinoxes). The semiannual variations in auroral precipitation can be explained by the R-M effect together with the equinoctial effect, which has been discussed by *Emery et al.* [2011]. We will focus our investigation on the annual variations in E_{PAR} and auroral precipitation. We apply a band-pass filter to E_{PAR} and auroral precipitation. The band-pass filter is centered at 365 days, with half-power points at 365 ± 20 days. Band-pass-filtered annual variations in E_{PAR} and auroral precipitation are shown in Figures 4a and 4b, respectively. As we can see, the annual variation in E_{PAR} is strongest during declining phase of solar cycle 23 (2002–2004) and the annual maxima occurs in early winter, with two exceptions in 1995 and 1996 when the annual maxima occurs in spring. This is consistent with *Newell et al.* [2013], who found that almost all reasonable solar wind driving functions peak in November and suggested that it is simply due to a combination of the R-M effect and the noncircular orbit of the Earth. The annual variations in HPe and HPi are similar to that in E_{PAR}, but the phase is shifted slightly later, which might be partly due to the modulation of the inclination of Earth's dipole axis to the rotation axis [see *Cliver et al.*, 2000]. The corresponding annual variation in the ionospheric conductivity would be expected and may contribute to the observed annual variations in the IL index and WEJ in Sector 1, because the conductivity in the midnight sector is mainly determined by particle precipitation. In fact, the annual perturbations in the IL index and WEJ in Sector 1 correspond well with the perturbations in HPe and HPi (cf. Figures 2 and 4b). On the other hand, because the convection electric field is closely associated with the IMF *By* and *Bz* components and solar wind speed [see *Weimer*, 1996, 2005; *Ridley et al.*, 2000; *Matsuo et al.*, 2002], it should show a similar annual variation as that of parallel electric field E_{PAR} and also contribute to the annual variations in the IL index and WEJ in Sector 1.

In order to further examine the relative importance of the convective electric field and the conductivity associated with particle precipitation in causing the annual variations in the IL index and WEJ in Sector 1 (2200–0100 MLT), we proceed with a cross-correlation analysis. Considering that electrons are dominant

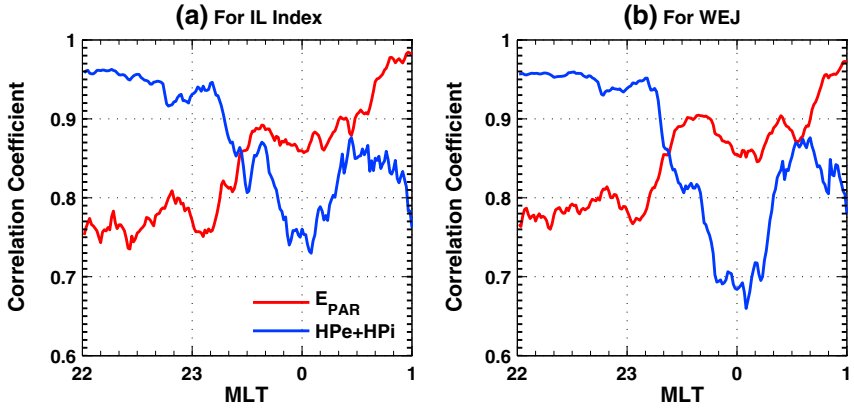

Figure 5. MLT variation of correlation coefficient (r) obtained from the zero-lag cross correlation of band-pass-filtered annual perturbations in (a) the IL index and (b) WEJ with the perturbations in E_{PAR} and auroral precipitation (HPe + HPi) during 1995–2009.

in auroral precipitation [*Guo et al.*, 2011], and the annual variation of HPe is significantly stronger than that of HPi (cf. Figure 4), we examine the total particle precipitation (HPe + HPi) instead of each separately. The band-pass-filtered annual perturbations in the IL index and WEJ in each MLT bin are cross correlated with the perturbations in E_{PAR} and auroral precipitation (HPe + HPi), and the zero-lag correlation coefficients (r) are plotted in Figure 5 (all the correlations are significant). The correlation coefficients reveal an obvious feature: auroral precipitation correlates better with the IL index and WEJ in the MLT sector ~2200–2320, whereas E_{PAR} does in the MLT sector ~2320–0100. This may imply that the conductivity associated with particle precipitation plays a more important role in producing annual variations in the IL index and WEJ in the MLT sector ~2200–2320, while the convective electric field does in the MLT sector ~2320–0100. However, to quantify the relative contribution of the conductivity and the convective electric field, additional data sources such as the convective electric field data and model simulations would be required.

As discussed above, the observed annual variations in the IL index and WEJ in Sector 1 suggest they are caused by both the convective electric field and the conductivity associated with particle precipitation, and those in Sector 3 suggest they are caused by solar EUV conductivity effect and the equinoctial effect. As Sector 2 is between Sector 1 and Sector 3, the annual variations in Sector 2 might be attributed to the combination of annual variations caused by these effects which maximize in different seasons. In this way, we can explain the relatively weak annual variations in Sector 2 (cf. Figure 2). As mentioned earlier, the periods of ~400 days might be the signals of annual variations. To examine the annual variations including the periods of ~400 days, we apply a band-pass filter with half-power points at periods of 345 and 425 days to each MLT bin of IL index and WEJ. The results (not shown) suggest that the annual variations in Sector 2 are quite similar to those shown in Figure 2 (with period between 345 and 385 days), except for their relatively larger amplitudes. Moreover, they are still weak when compared to those in Sector 1 and Sector 3. Therefore, the

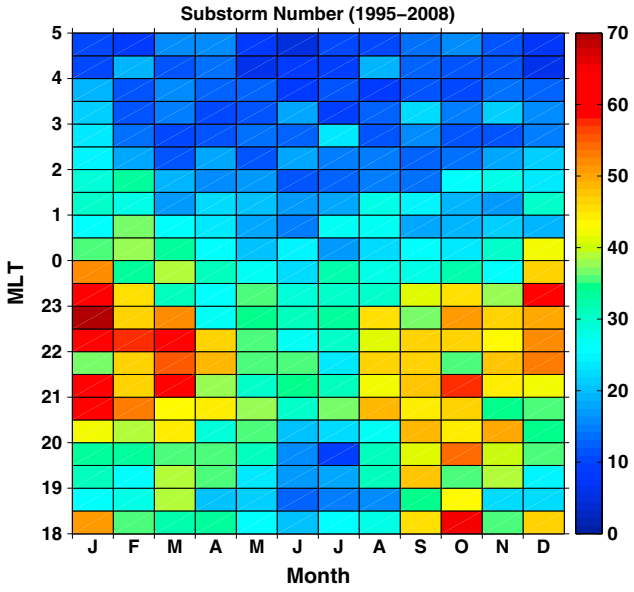

Figure 6. Seasonal and MLT variations of the number of substorms from 1995 to 2008.

annual variations in Sector 2 including the periods of ~400 days still can be explained by the combined effects of annual variations caused by all the previously mentioned effects.

3.2. Annual Variation in Substorm Occurrence Rate

Figure 6 shows the seasonal and MLT variations of the number of substorms for the period 1995–2008. A total of 7541 substorms from the substorm list identified by *Tanskanen* [2009] utilizing the IL index in the time interval between 1600 and 0300 UT (1800–0500 MLT)are used. As we can see, the substorms occur mainly in the premidnight region, roughly 2000–0000 MLT, with maxima during the winter and equinox months and minima during the summer months, implying an annual variation in substorm occurrence rate.

It is interesting to note that the annual variation in substorm occurrence rate is in good agreement with the annual variations in the IL index and WEJ in the midnight sector, which are associated with the annual variation in the solar wind driving (from parallel electric field E_{PAR}). Therefore, it is reasonable to suggest that the elevated solar wind driving during the winter months may make a contribution to the higher substorm occurrence in winter. This suggestion is well supported by the idea of *Morley and Freeman* [2007] that substorms require initial elevated solar wind driving.

4. Conclusion

The results in the present paper are the first to reveal the annual variation in the westward electrojet using the IMAGE network magnetic measurements. The observed annual variation in the westward electrojet shows strong MLT dependence owing to the different sources. In the MLT sector 2200–0100, the annual variations with maxima in winter suggest they are caused by the combined effects of the convective electric field and the conductivity associated with particle precipitation. Furthermore, the conductivity seems to play a more important role in the MLT sector ~2200–2320, while the convective electric field appears to be more important in the MLT sector ~2320–0100. In the MLT sector 0300–0600, the annual variations with maxima in summer suggest they are caused by solar EUV conductivity effect and the equinoctial effect, which work in two fundamentally different ways. The solar EUV conductivity effect works by increasing ionospheric conductivity and enhancing the westward electrojet in summer, while the equinoctial effect works by decreasing solar wind-magnetosphere coupling efficiency and weakening the westward electrojet in winter. In the MLT sector 0100–0300, the annual variations are relatively weak and can be attributed to the combined effects of annual variations caused by all the previously mentioned effects.

It is also found that a significant annual variation in substorm occurrence rate, mainly occurring in the premidnight region, is similar to that in the westward electrojet associated with solar wind driving. We suggest that elevated solar wind driving during the winter months can make a contribution to higher substorm occurrence in winter in the Northern Hemisphere.

Acknowledgments

This work is jointly supported by the Chinese Academy of Sciences (KZZD-EW-01-4), the 973 program (2012CB825601), the National Natural Science Foundation of China (41031066, 41231068, and 41374187), and the Specialized Research Fund for State Key Laboratories. J. Guo thanks the support by the NICT International Exchange Program. H. Liu acknowledges support by JSPS Grant-in-Aid for scientific research (B) (25800274) and Shisedo Science grant. ET acknowledges the financial support by EU/FP7 ESPAS and the Academy of Finland to the ReSoLVE Centre of Excellence (272157). We thank the institutes who maintain the IMAGE Magnetometer Array. The Northern Hemisphere electron and ion hemispheric power (HPe and HPi) estimates are taken from the coupling energetics and dynamics of atmospheric regions (CEDAR) database, which is supported by the National Science Foundation. NCAR is sponsored by the National Science Foundation (B. Emery).

Yuming Wang thanks Boris Kozelov and an anonymous reviewer for their assistance in evaluating this paper.

References

Ahn, B.-H., B. Emery, H. Kroehl, and Y. Kamide (1999), Climatological characteristics of the auroral ionosphere in terms of electric field and ionospheric conductance, *J. Geophys. Res.*, *104*(A5), 10,031–10,040.

Ahn, B.-H., H. Kroehl, Y. Kamide, and E. Kihn (2000), Seasonal and solar cycle variations of the auroral electrojet indices, *J. Atmos. Sol. Terr. Phys.*, *62*, 1301–1310.

Amm, O., and A. Viljanen (1999), Ionospheric disturbance magnetic field continuation from the ground to the ionosphere using spherical elementary current systems, *Earth Planets Space*, *51*, 431–440.

Cliver, E. W., Y. Kamide, and A. G. Ling (2000), Mountains versus valleys: Semiannual variation of geomagnetic activity, *J. Geophys. Res.*, *105*, 2413–2424.

Davis, T. N., and M. Sugiura (1966), Auroral electrojet activity index AE and its universal time variations, *J. Geophys. Res.*, *71*(3), 785–801, doi:10.1029/JZ071i003p00785.

Emery, B. A., V. Coumans, D. S. Evans, G. A. Germany, M. S. Greer, E. Holeman, K. Kadinsky-Cade, R. J. Rich, and W. Xu (2008), Seasonal, Kp, solar wind, and solar flux variations in long-term single-pass satellite estimates of electron and ion auroral hemispheric power, *J. Geophys. Res.*, *113*, A06311, doi:10.1029/2007JA012866.

Emery, B. A., I. G. Richardson, D. S. Evans, R. J. Rich, and W. Xu (2009), Solar wind structure sources and periodicities of global electron hemispheric power over three solar cycles, *J. Atmos. Sol. Terr. Phys.*, *71*, 1157–1175, doi:10.1016/j.jastp.2008.08.005.

Emery, B. A., I. G. Richardson, D. S. Evans, R. J. Rich, and G. R. Wilson (2011), Solar rotational periodicities and the semiannual variation in the solar wind, radiation belt, and aurora, *Sol. Phys.*, *274l*, 399–425, doi:10.1007/s11207-011-9758-x.

Finch, I. D., M. L. Lockwood, and A. P. Rouillard (2008), Effects of solar wind magnetosphere coupling recorded at different geomagnetic latitudes: Separation of directly driven and storage/release systems, *Geophys. Res. Lett.*, *35*, L21105, doi:10.1029/2008GL035399.

Guo, J., X. Feng, B. A. Emery, J. Zhang, C. Xiang, F. Shen, and W. Song (2011), Energy transfer during intense geomagnetic storms driven by interplanetary coronal mass ejections and their sheath regions, *J. Geophys. Res.*, *116*, A05106, doi:10.1029/2011JA016490.

Guo, J., X. Feng, T. I. Pulkkinen, E. I. Tanskanen, W. Xu, J. Lei, and B. A. Emery (2012), Auroral electrojets variations caused by recurrent high-speed solar wind streams during the extreme solar minimum of 2008, *J. Geophys. Res.*, *117*, A04307, doi:10.1029/2011JA017458.

Kallio, E. I., T. I. Pulkkinen, H. E. J. Koskinen, A. Viljanen, J. A. Slavin, and K. Ogilvie (2000), Loading-unloading processes in the nightside ionosphere, *Geophys. Res. Lett.*, *27*(11), 1627–1630, doi:10.1029/1999GL003694.

Kauristie, K., T. I. Pulkkinen, R. J. Pellinen, and H. J. Opgenoorth (1996), What can we tell about the AE-index from a single meridional magnetometer chain?, *Ann. Geophys.*, *14*, 1177–1185.

Lomb, N. R. (1976), Least-squares frequency analysis of unequally spaced data, *Astrophys. Space Sci.*, *39*, 447–462.

Lyatsky, W., P. T. Newell, and A. Hamza (2001), Solar illumination as cause of the equinoctial preference for geomagnetic activity, *Geophys. Res. Lett.*, *28*, 2353–2356, doi:10.1029/2000GL012803.

Matsuo, T., A. D. Richmond, and D. W. Nychka (2002), Modes of high-latitude electric field variability derived from DE-2 measurements: Empirical Orthogonal Function (EOF) analysis, *Geophys. Res. Lett.*, *29*(7), 11-1–11-4, doi:10.1029/2001GL014077.

McPherron, R. L., D. N. Baker, T. I. Pulkkinen, T. S. Hsu, J. Kissinger, and X. Chu (2013), Changes in solar wind-magnetosphere coupling with solar cycle, season, and time relative to stream interfaces, *J. Atmos. Sol. Terr. Phys.*, *99*, 1–13, doi:10.1016/j.jastp.2012.09.003.

Morley, S. K., and M. P. Freeman (2007), On the association between northward turnings of the interplanetary magnetic field and substorm onsets, *Geophys. Res. Lett.*, *34*, L08104, doi:10.1029/2006GL028891.

Newell, P. T., T. Sotirelis, J. P. Skura, C.-I. Meng, and W. Lyatsky (2002), Ultraviolet insolation drives seasonal and diurnal space weather variations, *J. Geophys. Res.*, *107*(A10), 1305, doi:10.1029/2001JA000296.

Newell, P. T., and J. W. Gjerloev (2011), Evaluation of SuperMAG auroral electrojet indices as indicators of substorms and auroral power, *J. Geophys. Res.*, *116*, A12211, doi:10.1029/2011JA016779.

Newell, P. T., J. W. Gjerloev, and E. J. Mitchell (2013), Space climate implications from substorm frequency, *J. Geophys. Res. Space Physics*, *118*, 6254–6265, doi:10.1002/jgra.50597.

Pulkkinen, A., et al. (2003), Ionospheric equivalent current distributions determined with the method of spherical elementary current systems, *J. Geophys. Res.*, *108*(A2), 1053, doi:10.1029/2001JA005085.

Pulkkinen, T. I., M. Palmroth, H. E. J. Koskinen, T. V. Laitinen, C. C. Goodrich, V. G. Merkin, and J. G. Lyon (2010), Magnetospheric modes and solar wind energy coupling efficiency, *J. Geophys. Res.*, *115*, A03207, doi:10.1029/2009JA014737.

Pulkkinen, T. I., E. I. Tanskanen, A. Viljanen, N. Partamies, and K. Kauristie (2011), Auroral electrojets during deep solar minimum at the end of solar cycle 23, *J. Geophys. Res.*, *116*, A04207, doi:10.1029/2010JA016098.

Ridley, A. J., G. Crowley, and C. Freitas (2000), An empirical model of the ionospheric electric potential, *Geophys. Res. Lett.*, *27*(22), 3675–3678.

Ridley, A. J., T. I. Gombosi, and D. L. DeZeeuw (2004), Ionospheric control of the magnetospheric configuration: Conductance, *Ann. Geophys.*, *22*, 567–584.

Russell, C. T., and R. L. McPherron (1973), Semiannual variation of geomagnetic activity, *J. Geophys. Res.*, *78*, 92–108.

Scargle, J. D. (1982), Studies in astronomical time series analysis. II. Statistical aspects of spectral analysis of unevenly spaced data, *Astrophys. J.*, *263*, 835–853.

Singh, A. K., R. Rawat, and B. M. Pathan (2013), On the UT and seasonal variations of the standard and SuperMAG auroral electrojet indices, *J. Geophys. Res. Space Physics*, *118*, 5059–5067, doi:10.1002/jgra.50488.

Svalgaard, L. (1977), Geomagnetic activity: Dependence on solar wind parameters, in *Coronal Holes and High Speed Wind Streams*, edited by J. B. Zirker, pp. 371, Colorado Associated University Press, Boulder, Colo.

Tanskanen, E. I. (2009), A comprehensive high-throughput analysis of substorms observed by IMAGE magnetometer network: Years 1993–2003 examined, *J. Geophys. Res.*, *114*, A05204, doi:10.1029/2008JA013682.

Tanskanen, E. I., T. I. Pulkkinen, A. Viljanen, K. Mursula, N. Partamies, and J. A. Slavin (2011), From space weather toward space climate time scales: Substorm analysis from 1993 to 2008, *J. Geophys. Res.*, *116*, A00I34, doi:10.1029/2010JA015788.

Weimer, D. R. (1996), A flexible IMF dependent model of high-latitude electric potentials having "Space Weather" applications, *Geophys. Res. Lett.*, *23*(18), 2549–2552.

Weimer, D. R. (2005), Improved ionospheric electrodynamic models and application to calculating Joule heating rates, *J. Geophys. Res.*, *110*, A05306, doi:10.1029/2004JA010884.

Zhao, H., and Q.-G. Zong (2012), Seasonal and diurnal variation of geomagnetic activity: Russell-McPherron effect during different IMF polarity and/or extreme solar wind conditions, *J. Geophys. Res.*, *117*, A11222, doi:10.1029/2012JA017845.